NACA

RESEARCH MEMORANDUM

THE EFFECT OF INLET INSTALLATION ON THE ZERO-LIFT DRAG OF A 60° DELTA-WING—BODY CONFIGURATION FROM FLIGHT TESTS AT MACH NUMBERS FROM 0.8 TO 1.86

By Charles F. Merlet

Langley Aeronautical Laboratory
Langley Field, Va.

NATIONAL ADVISORY COMMITTEE FOR AERONAUTICS

WASHINGTON

December 15, 1955

NACA RM L55I09

NATIONAL ADVISORY COMMITTEE FOR AERONAUTICS

RESEARCH MEMORANDUM

THE EFFECT OF INLET INSTALLATION ON THE ZERO-LIFT DRAG OF A 60° DELTA-WING—BODY CONFIGURATION FROM FLIGHT TESTS AT MACH NUMBERS FROM 0.8 TO 1.86

By Charles F. Merlet

SUMMARY

Zero-lift drag results are presented for two 60° delta-wing configurations employing air inlets. One model had twin conical-shock semicircular scoops installed just ahead of the wing-body juncture. In the other model, the wing section was modified over the inboard portion of the wing to allow installation of modified triangular inlets in the wing leading edge. Mass-flow ratios of 0.72 to 0.90 for the conical-shock inlets and from 0.94 to 0.79 for the wing-root inlets were obtained over a Mach number range from 0.8 to 1.86 and a Reynolds number range from 10×10^6 to 30×10^6.

The drag of the configuration using the conical-shock scoops was higher than the drag of the wing-root-inlet configuration throughout the Mach number range. A comparison of the inlet configurations with the basic wing-body configuration indicated that installation of the inlets increased the drag coefficients at subsonic and transonic speeds, while decreasing the drag-rise Mach number. At Mach numbers greater than 1.2, it appeared that the increase in drag coefficient due to the installation of the conical-shock inlets was largely due to spillage drag, while the wing-root-inlet configuration had an external drag coefficient equal to or less than that of the basic wing-body model.

INTRODUCTION

As part of its research program on air inlets, the Pilotless Aircraft Research Division of the Langley Aeronautical Laboratory is currently conducting a free-flight investigation to determine the effects of the installation of inlets on airplane configurations. Data are presented in reference 1 for two versions of a supersonic swept-wing interceptor configuration equipped with an inlet designed to supply air to a

single engine. The investigation reported herein was conducted on a design suitable for a multiengine airplane, such as a high-altitude supersonic bomber.

The basic wing-body combination selected was a low-drag configuration of reference 2, and consisted of a 60° delta wing having an NACA 65A006 airfoil section parallel to the free-stream direction, mounted on a parabolic body of revolution. This basic wing-body combination was modified to allow the installation of inlets and ducting suitable for a multiengine configuration. Because of the center-of-gravity location of the design airplane, the wing was located about 0.14 mean aerodynamic chord rearward of its position on the basic wing-body configuration, so that the trailing edge intersected the base of the body. In keeping with the idea of testing airplane configurations, the twin vertical fins used in reference 2 were replaced by a single vertical 60° delta fin.

Two models were tested, each utilizing a different type of inlet. One model had semicircular twin scoop inlets of the conical-shock type installed just ahead of the wing leading edge. The other model had twin modified triangular inlets installed in the leading edge of the wing. The tests were made with rocket-propelled models in free flight at the Langley Pilotless Aircraft Research Station at Wallops Island, Va. Data are presented for a Mach number range from 0.8 to 1.86.

SYMBOLS

A	cross-sectional area, sq in.
C_D	drag coefficient, $\frac{\text{Drag}}{\frac{\gamma}{2} pM^2S}$
c	chord, in.
l	model length, 65 in.
M	Mach number
m/m_o	ratio of duct mass flow to the mass flow through a free-stream tube having an area equal to the projected frontal area of the inlet
p	static pressure, lb/sq ft
R	Reynolds number

[redacted]

S	total wing area, 7.567 sq ft
t	thickness, in.
x	axial distance measured from tip of model nose, in.
x'	axial distance measured from leading edge of wing, in.
γ	ratio of specific heats, 1.40 for air
θ_l	cowling position parameter (angle between vertex of cone and lip of inlet)

Subscripts:

B	base
D	duct
T	total
i	inlet
int	internal

MODELS

Photographs of the models are presented in figure 1, and sketches are presented in figure 2. Both models were derived from the same basic configuration, model 5 of reference 2, consisting of a 60° delta wing with an NACA 65A006 airfoil section parallel to the free stream, mounted on a parabolic body of revolution (table I). The present models were made one-half the scale of the model of reference 2 and equipped with an internal sustainer rocket motor to increase the maximum Mach number of the tests. The wing was moved rearward about 0.14 mean aerodynamic chord, so that the trailing edge passed through the base of the body. A single 60° delta fin having an NACA 65A004 airfoil section parallel to the free stream was mounted vertically at the rear of the body to furnish directional stability.

Model 1 (fig. 2(a)) had a conical-shock inlet on each side of the body just rearward of the maximum body diameter and ahead of the wing leading edge. Details of the inlet, its installation, and the ducting are shown in figure 3(a). The inner body, a 25° half-angle cone positioned with a value of $\theta_l = 42.5°$, was mounted on a boundary-layer splitter plate which was concentric with the body and swept from the tip

[redacted]

of the cone to the inlet lip. The splitter plate was separated from the body by a 3/8-inch-high boundary-layer diverter with an initial total angle of 40°.

The inlet had internal and external cowl-lip angles of 0° and 17°, respectively. The minimum duct area was at the inlet station and was 0.73 of the inlet capture area. The inlet capture area (for both inlets of model 1) was 9.60 square inches. Each inlet was faired into its own semisubmerged nacelle which housed the individual ducting and ended in an individual exit at the base of the model, as shown in figure 3(a). The variation of duct area along the length of the model is presented in figure 4. Externally, the surfaces of the semisubmerged nacelles were parallel to the free-stream direction from the wing leading edge to a point 4 inches forward of the trailing edge. The last 4 inches were boattailed with an angle of 4.4°. Coordinates of the external contours of the ducting are presented in table II.

Model 2 had modified triangular-shaped inlets located in the leading edge of each wing. Space for the inlets was provided by modifying the inboard section of the wing as shown in table III. The modification was achieved by providing a constant 6-percent-thick section along the theoretical root chord from the 5-percent-chord point to the 70-percent-chord point. Ahead of the 40-percent-chord line, the inboard section was modified only over the portion of the span that enclosed the inlet ducting, 8.20 inches from the body center line. This portion of the modified airfoil was defined by joining the root section to the modified section 8.20 inches from the model center line (see table III) with straight-line elements along constant values of x/c. The resulting discontinuity in wing thickness at this spanwise station was faired arbitrarily. Rearward from the 40-percent-chord line to the trailing edge, the airfoil shape was modified 10.5 inches out from the model center line. The external contour in this region was formed by joining the modified root-chord airfoil section of table III to the standard airfoil shape by straight-line elements along any constant value of x/c.

Details of the inlet and ducting are shown in figure 3(b). The inlet lips, which were internally rounded, were staggered by reducing the sweep angle of the lower lip to 57°. The resulting stagger angle varied with span from 42.25° at the inboard end to 38.42° outboard. The projected frontal area of both inlets was 9.10 square inches. The floor of the duct was raised 3/8 inch from the body by a boundary-layer diverter having an initial angle of 50°. Beginning at a point just downstream of the lip, the floor of the duct was parallel to the body center line until the entering airflow was completely enclosed. Transition was then made to a section similar to that of model 1 by curving the duct center line and increasing the duct width. The longitudinal variation of duct area is presented in fig. 4.

[redacted]

Externally, the portion of the ducting of model 2 that exceeded the wing thickness was enclosed by a fairing, beginning at fuselage station 31.2 and extending to the base of the model. The last 11 inches of this fairing were identical to that of model 1. External coordinates of the fairing are presented in table II.

For both models, the duct exits were made larger than the minimum area of the inlet to insure achievement of maximum mass-flow rates. The exit areas for both ducts totaled 8.16 square inches for model 1 and 8.83 square inches for model 2. The base areas were 20.80 square inches and 20.13 square inches for models 1 and 2, respectively. The longitudinal area distributions of the models, adjusted for the mass-flow rate at $M = 1.0$, are presented in figure 5. The area deducted for the mass-flow rate is shown at the bottom of the figure. The area distribution of the basic wing-body model of reference 2 is also shown for comparison.

INSTRUMENTATION AND TESTS

Each model was equipped with an accelerometer which measured longitudinal deceleration, a manifold total-pressure rake to measure duct total pressure, a static-pressure orifice to measure duct-exit static pressure, and six static orifices manifolded together to determine base pressure. The locations of the pressure rake and orifices are indicated in figure 3. A four-channel telemeter transmitted continuous time histories of these data to ground receiving stations throughout the flight. Model velocity was determined from a CW Doppler radar velocimeter. The model's position in space was determined from measurements made by an NACA modified SCR-584 radar tracking unit. Ambient air conditions were determined from radiosonde measurements made at the conclusion of each of the flight tests.

The models were boosted to a Mach number of approximately 1.4 by a single Deacon rocket motor. Following the boost period, a $3\frac{1}{4}$-inch rocket motor contained in the body accelerated the models to their maximum Mach number of about 1.9. All data were obtained during the coasting flight that followed the second boost period as the model decelerated to subsonic speeds along a nearly zero-lift flight path. The Reynolds numbers (based on wing mean aerodynamic chord of 2.42 feet) that were encountered are shown in figure 6.

ANALYSIS OF DATA

The total drag coefficient was obtained from reduction of the accelerometer data. Decelerations determined from the differentiation of the

curve for Doppler velocity plotted against time were used to check the accelerometer data. For model 2, comparison of the two total-drag curves indicated discrepancies in the telemeter data at subsonic and transonic speeds. The telemeter data for this model were therefore corrected to agree with decelerations obtained from Doppler radar measurements.

The internal drag, defined as the momentum difference between flow conditions in the free stream and at the model exit (ref. 3), was determined from the duct internal-pressure measurements, as were the mass-flow ratios. The duct-exit total pressure, which was assumed to be equal to the total pressure measured by the duct manifold total-pressure rake, was used with the measured exit static pressure to determine the exit Mach number of the duct. Mass-flow ratios and internal drag were then calculated by using these determined exit conditions. Base drag was calculated by assuming that the average base pressure measured by the manifold orifices applied over the entire base area. The external drag was then calculated by subtracting the internal and base drag from the total drag.

RESULTS AND DISCUSSION

The total, internal, and base drag coefficients for each model are presented in figure 7 as a function of Mach number. The abrupt peaks that occur in both the total and base drag coefficients in the Mach number range from 1.3 to 1.6 are associated with afterburning of the internal rocket motor. This intermittent burning of residue of the rocket grain caused a slight flow out of the rocket nozzle, which affected the base pressure significantly without producing any measurable thrust. Examination of the data shows that the increment in total drag is entirely accounted for by the measured increment in base drag.

Mass-flow ratios determined from flight measurements are presented on figure 8. For model 1, the mass-flow ratios at Mach numbers greater than 1.5 are somewhat lower than those of a comparable nose inlet, because the inlet is located in a region where the local flow has been expanded over free-stream conditions. Although the inlet lip angles are such as to cause a detached shock ahead of the lip over most of the test Mach number range, the spillage associated with this detached shock appears to be small. The variation of mass-flow ratio with Mach number for model 2 is somewhat unusual. Considering the relative sizes of the reference inlet area, the minimum inlet area, and the exit (fig. 4), the mass-flow ratios at subsonic Mach numbers appear reasonable. As the Mach number increased, however, the mass-flow ratio decreased unexplainably, becoming approximately constant for Mach numbers greater than 1.5. For each model, the exit area was larger than the minimum inlet area and it is therefore believed that at supersonic speeds these mass-flow rates are the maximum attainable for the particular inlet geometry and location tested.

[redacted]

The external drag coefficients for both models are presented in figure 9 as a function of Mach number. Since both models are operating at maximum flow rates, the drag coefficients are a minimum for the configurations tested. The total drag minus base drag for the basic wing-body configuration reported in reference 2 is also shown, corrected to the average Reynolds number of the present tests. This correction added an increment in drag coefficient that varied from 0.0009 to 0.0007 between $M = 0.8$ and $M = 1.4$. A drag "bucket" occurred for all three models between Mach numbers of 0.95 and 0.96. The pressure drag over the boattail of the model of reference 4 showed a similar effect.

The external drag coefficient of model 1 exceeds that of model 2 throughout the Mach number range. At subsonic and low supersonic speeds, the difference in drag may be due in part to the difference in spillage drag associated with the different mass-flow ratios (fig. 8) for the two models at these speeds. As the Mach number increases, the mass-flow ratios become more comparable and hence the difference in drag appears to be a result of the difference in configurations.

Comparison of the drag results for the present models with those for model 5 of reference 2 (corrected to Reynolds numbers of present tests) indicates the effect on drag of installing the inlet on the basic wing-body configuration. In comparing these results, it should be noted that the installation of the inlet and ducting increased the wetted surface area of the configuration by about 5 percent of the total wing area. At subsonic and transonic speeds, the external drag coefficients of the inlet configurations were higher than the basic wing-body values. The inlet configurations also had lower drag-rise Mach numbers and greater transonic drag increases.

At supersonic speeds, model 1 had a consistently higher drag coefficient than the basic wing-body model. Data presented in reference 5 on the external drag of an RM-10 body equipped with two conical-shock scoop inlets show a comparable increase in drag over the body-alone drag. For example, at $M = 1.49$ the increase in drag (based on wing area of the present tests) is about 0.002. It appears reasonable, then, to assume that the higher supersonic drag level of model 1 is largely the result of an increased fuselage drag due to the installation of the inlets.

Model 2, on the other hand, had higher drag only up to a Mach number of 1.2. As the Mach number increased above this value, the decreasing values of drag coefficient suggest that installation of this inlet would not have increased the drag of the basic wing-body model. It appears that the modifications imposed on the configuration by the installation of the wing-root inlets had less effect on the supersonic drag than did the installation of the conical-shock inlets.

It should be noted that comparison of the external drag coefficients of the two inlet configurations does not allow complete evaluation of their relative worth. Proper consideration must be given to the effect of diffuser total-pressure recovery on the engine thrust characteristics. Since there was no external compression for the inlets of model 2, the conical-shock inlets of model 1 would be expected to have better total-pressure recovery than the wing-root inlet of model 2 at Mach numbers greater than 1.5. Thus, on the basis of thrust minus drag, the two configurations would appear more nearly equal.

SUMMARY OF RESULTS

Zero-lift drag data are presented for two 60° delta-wing configurations employing air inlets over a Mach number range from 0.8 to 1.86. One model had twin conical-shock inlets installed just ahead of the wing-body juncture, which operated at mass-flow ratios from 0.72 to 0.90 over the test Mach number range. The other model employed a pair of modified triangular inlets installed in the inboard portion of the wing leading edge, which operated at mass-flow ratios from 0.94 to 0.79 over the Mach number range. Comparison of the external drag results of the two inlet configurations and the basic wing-body drag results previously published produced the following results:

1. The drag of the configuration employing wing-root inlets was lower than that of the configuration with conical-shock inlets throughout the test Mach number range.

2. Installation of inlets resulted in higher drag at subsonic and transonic speeds as compared with the basic wing-body drag results.

3. At Mach numbers greater than 1.2, the external drag coefficient of the configuration with wing-root inlets was equal to or lower than the drag of the basic wing-body configuration, whereas the drag of the configuration with conical-shock inlets exceeded the drag of the basic wing-body configuration at supersonic speeds.

Langley Aeronautical Laboratory,
National Advisory Committee for Aeronautics,
Langley Field, Va., August 29, 1955.

[redacted]

REFERENCES

1. Judd, Joseph H.: A Free-Flight Investigation of the Drag Coefficients of Two Single-Engine Supersonic Interceptor Configurations From Mach Number 0.8 to 1.90 To Determine the Effect of Inlet and Engine Locations. NACA RM L55G05a, 1955.

2. Morrow, John D., and Nelson, Robert L.: Large-Scale Flight Measurements of Zero-Lift Drag of 10 Wing-Body Configurations at Mach Numbers From 0.8 to 1.6. NACA RM L52D18a, 1953.

3. Merlet, Charles F., and Putland, Leonard W.: Flight Determination of the Drag of Conical-Shock Nose Inlets with Various Cowling Shapes and Axial Positions of the Center Body at Mach Numbers From 0.8 to 2.0. NACA RM L54G21a, 1954.

4. Stoney, William E., Jr.: Pressure Distributions at Mach Numbers From 0.6 to 1.9 Measured in Free Flight on a Parabolic Body of Revolution With Sharply Convergent Afterbody. NACA RM L51L03, 1952.

5. Valerino, Alfred S., Pennington, Donald B., and Vargo, Donald J.: Effect of Circumferential Location on Angle of Attack Performance of Twin Half-Conical Scoop-Type Inlets Mounted Symmetrically on the RM-10 Body of Revolution. NACA RM E53G09, 1953.

[redacted]

TABLE I.- BASIC FUSELAGE COORDINATES

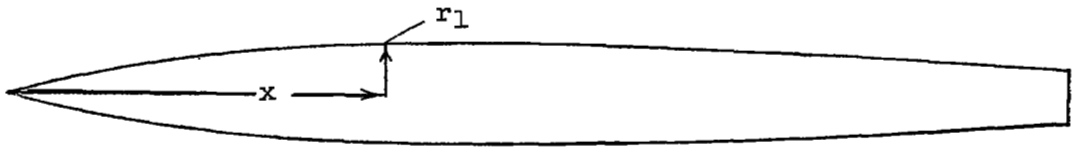

x, in.	r_1, in.
0	0
.390	.097
.585	.145
.975	.239
1.950	.469
3.900	.902
5.850	1.298
7.800	1.658
11.700	2.267
15.600	2.730
19.500	3.047
23.400	3.218
27.300	3.248
31.200	3.221
35.100	3.161
39.000	3.069
42.900	2.943
46.800	2.785
50.700	2.594
54.600	2.371
58.500	2.115
62.400	1.825
64.000	1.750
65.000	1.750

[redacted]

TABLE II.- EXTERNAL COORDINATES OF DUCT

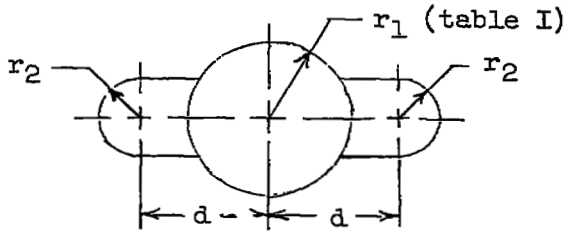

Model 1

x, in.	d, in.	r_2, in.
27.085	3.750	1.680
30.875	3.750	1.750
	|	|
61.0	3.750	1.750
Straight line taper		
65.0	3.750	1.442

Model 2

x, in.	d, in.	r_2, in.
31.2	1.471	1.750
Straight line taper		
52.0	3.640	1.750
54.0	3.750	1.750
61.0	3.750	1.750
Straight line taper		
65.0	3.750	1.442

[redacted]

TABLE III.- COORDINATES OF MODIFIED AIRFOIL SECTION OF MODEL 2

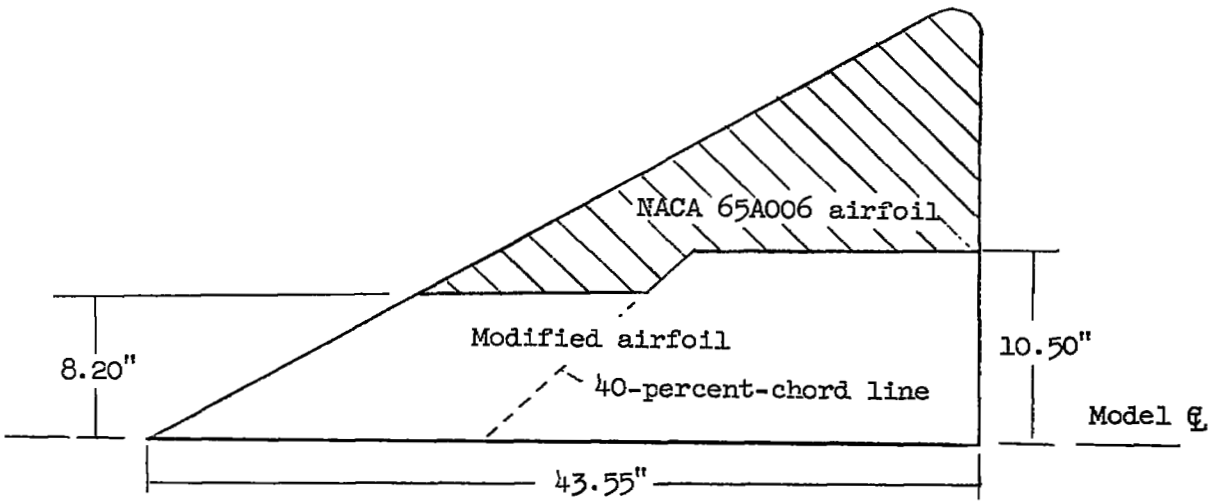

Root section

x'/c, percent chord	t/c, percent chord
0	2.46
.50	2.53
.75	2.60
1.25	2.69
2.50	2.89
5.00	3.00
70.00	3.00
75.00	2.91
80.00	2.62
85.00	2.09
90.00	1.45
95.00	0.75
100.00	0.02

Outboard section (8.20 inches from root chord)

x'/c, percent chord	t/c, percent chord
0	0.91
.50	1.00
.75	1.03
1.25	1.13
2.50	1.34
5.00	1.66
7.50	1.92
10.00	2.36
15.00	2.54
20.00	2.66
25.00	2.81
30.00	2.94
35.00	2.97
40.00	3.00

Downstream of 40-percent-chord line, external contour is formed by straight-line elements along constant chord line from root section to true airfoil section, 10.50 inches from root chord.

[redacted]

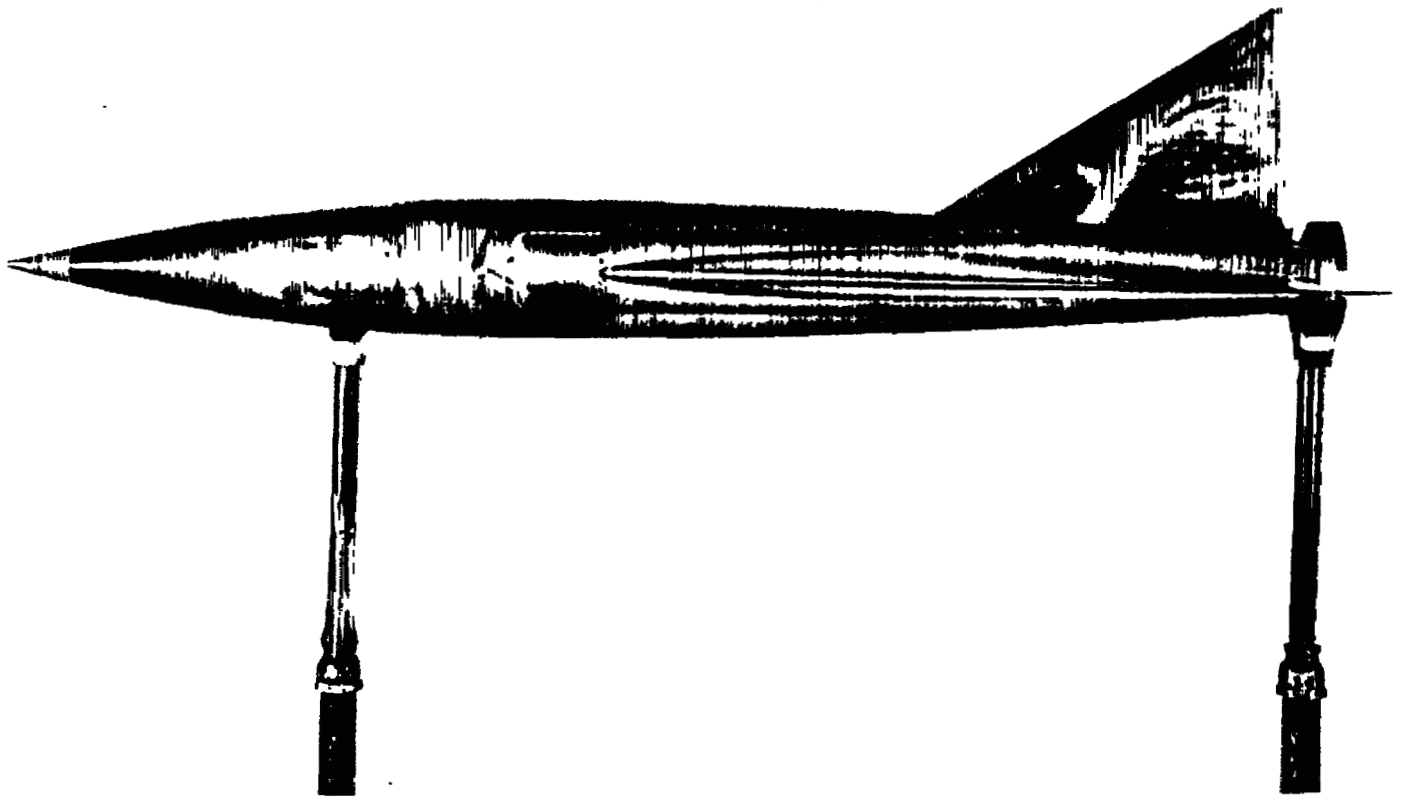

L-83541.1

(a) Side view of model 1.

Figure 1.- Photographs of the models.

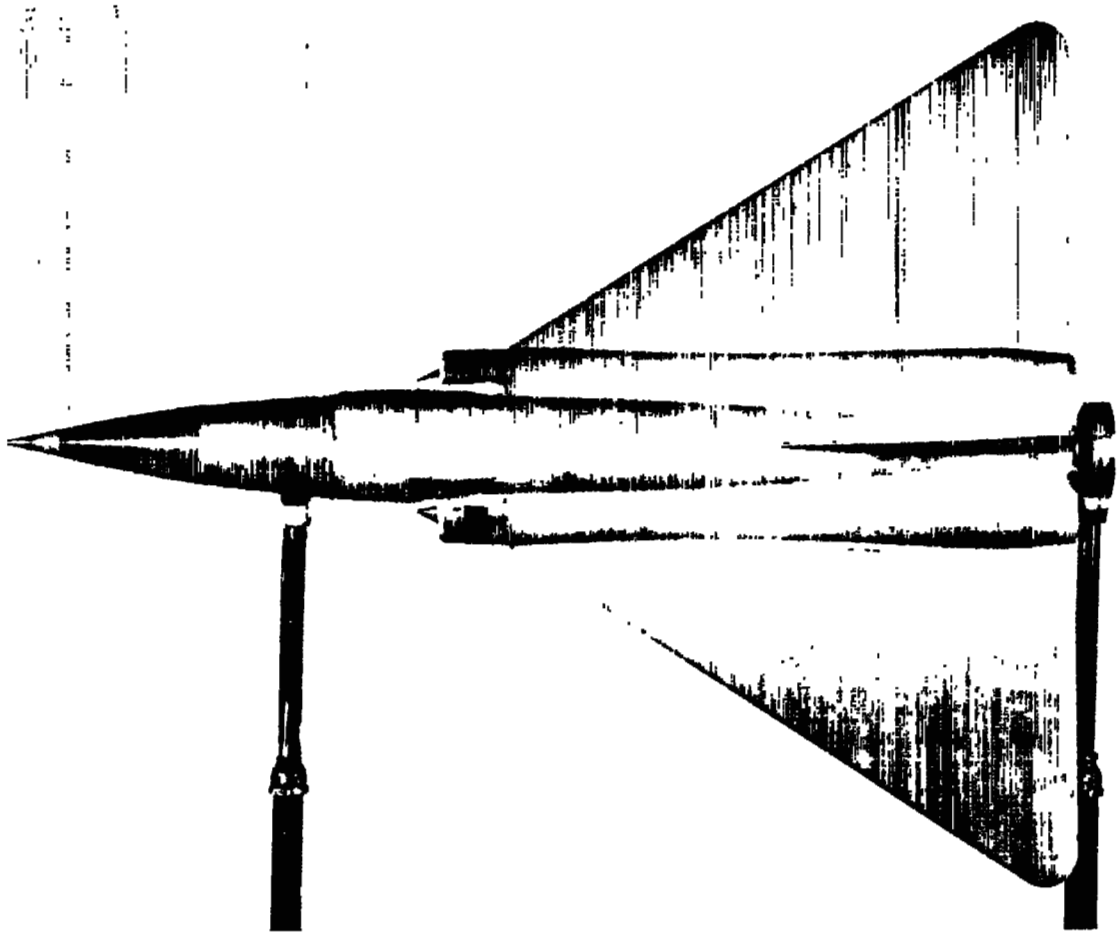

L-83539.1

(b) Top view of model 1.

Figure 1.- Continued.

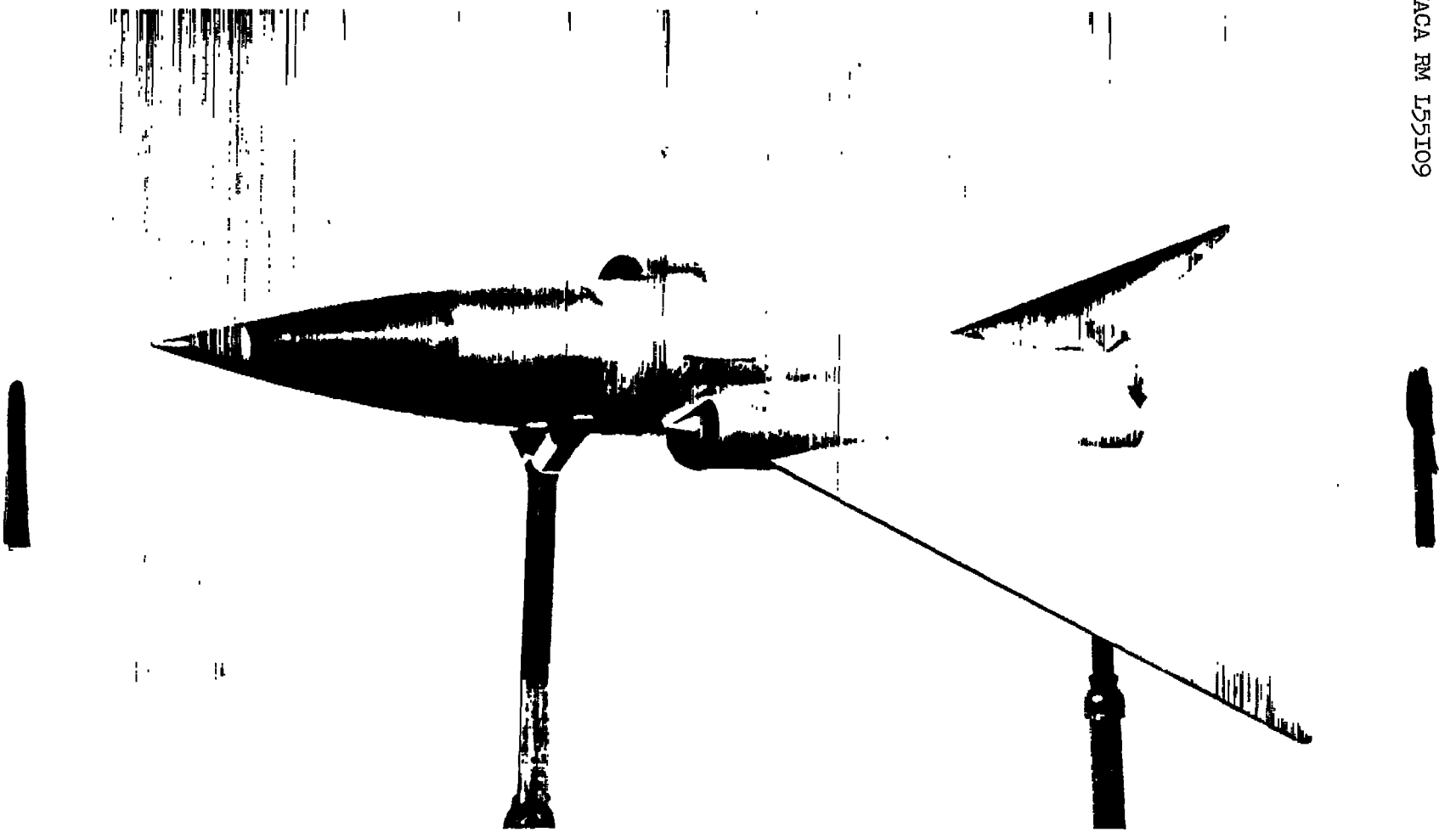

L-83540.1

(c) Three-quarter front view of model 1.

Figure 1.- Continued.

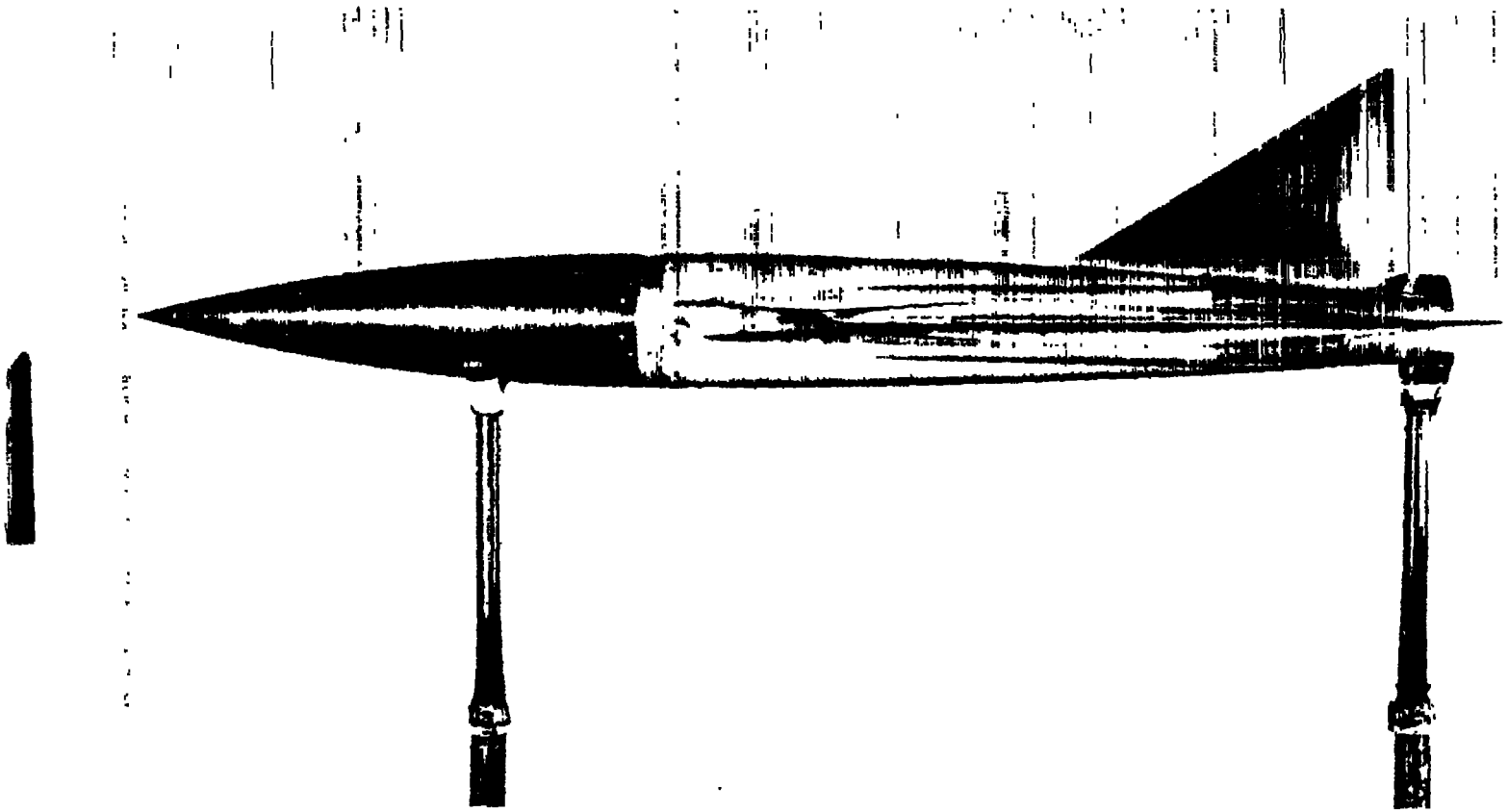

L-84661.1

(d) Side view of model 2.

Figure 1.- Continued.

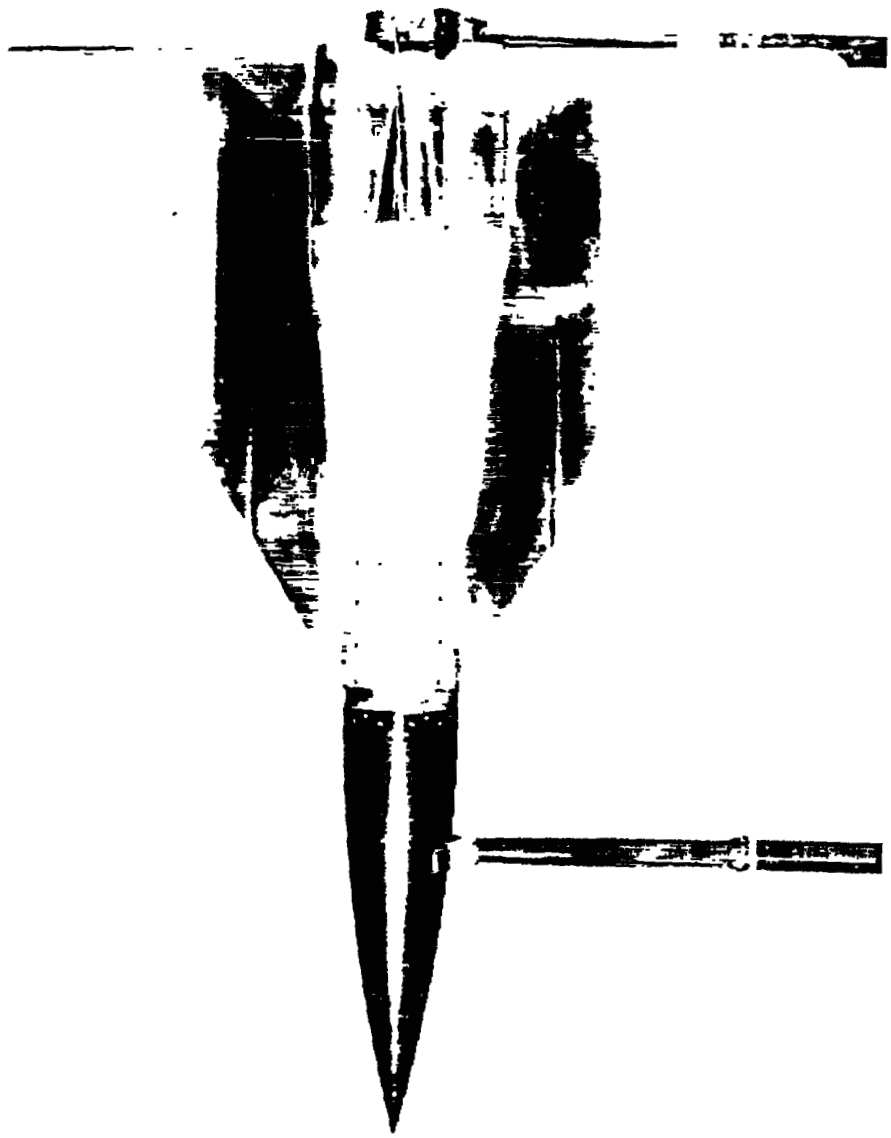

L-84662.1

(e) Top view of model 2.

Figure 1.- Continued.

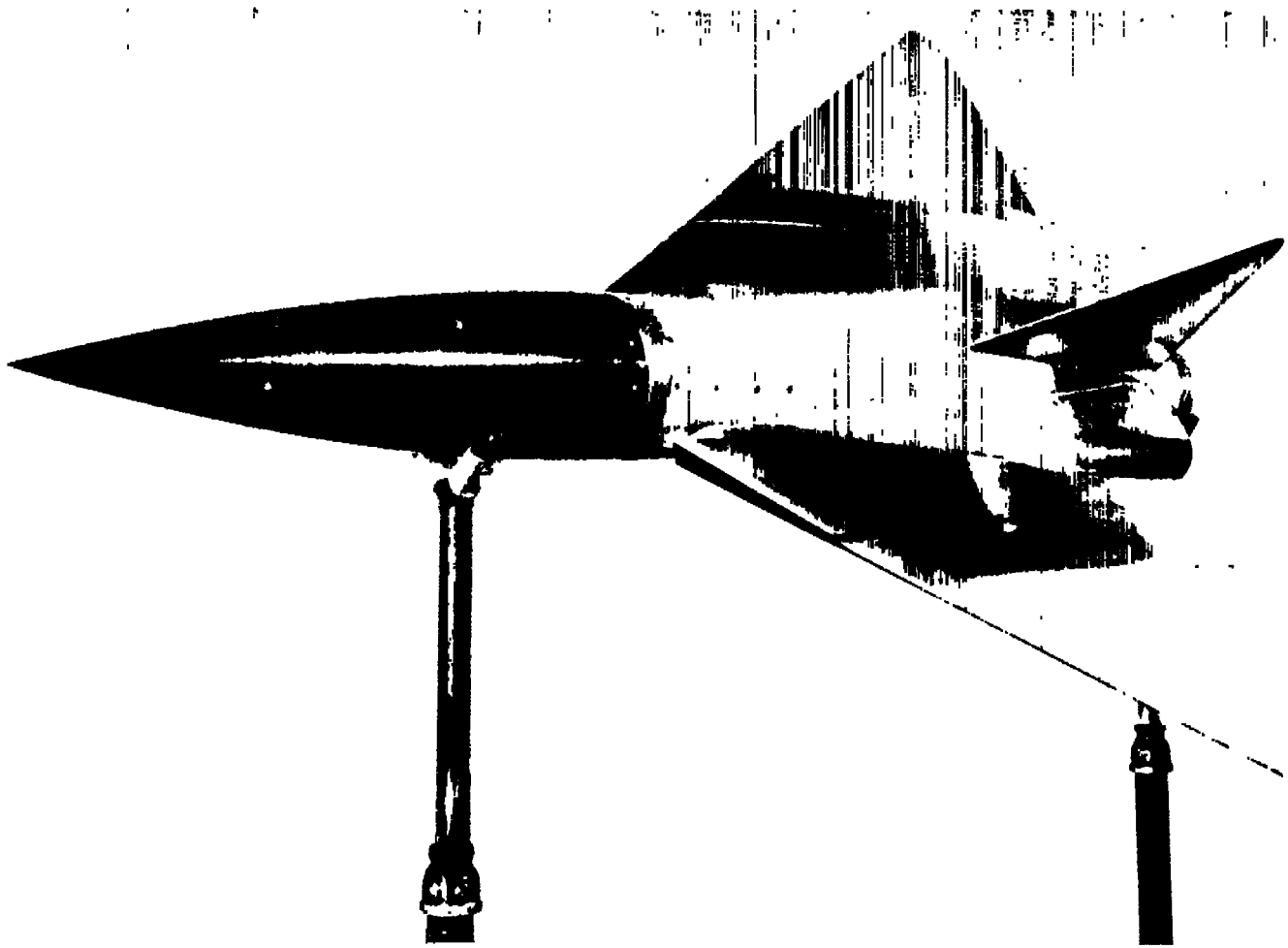

L-84663.1

(f) Three-quarter front view of model 2.

Figure 1.- Concluded.

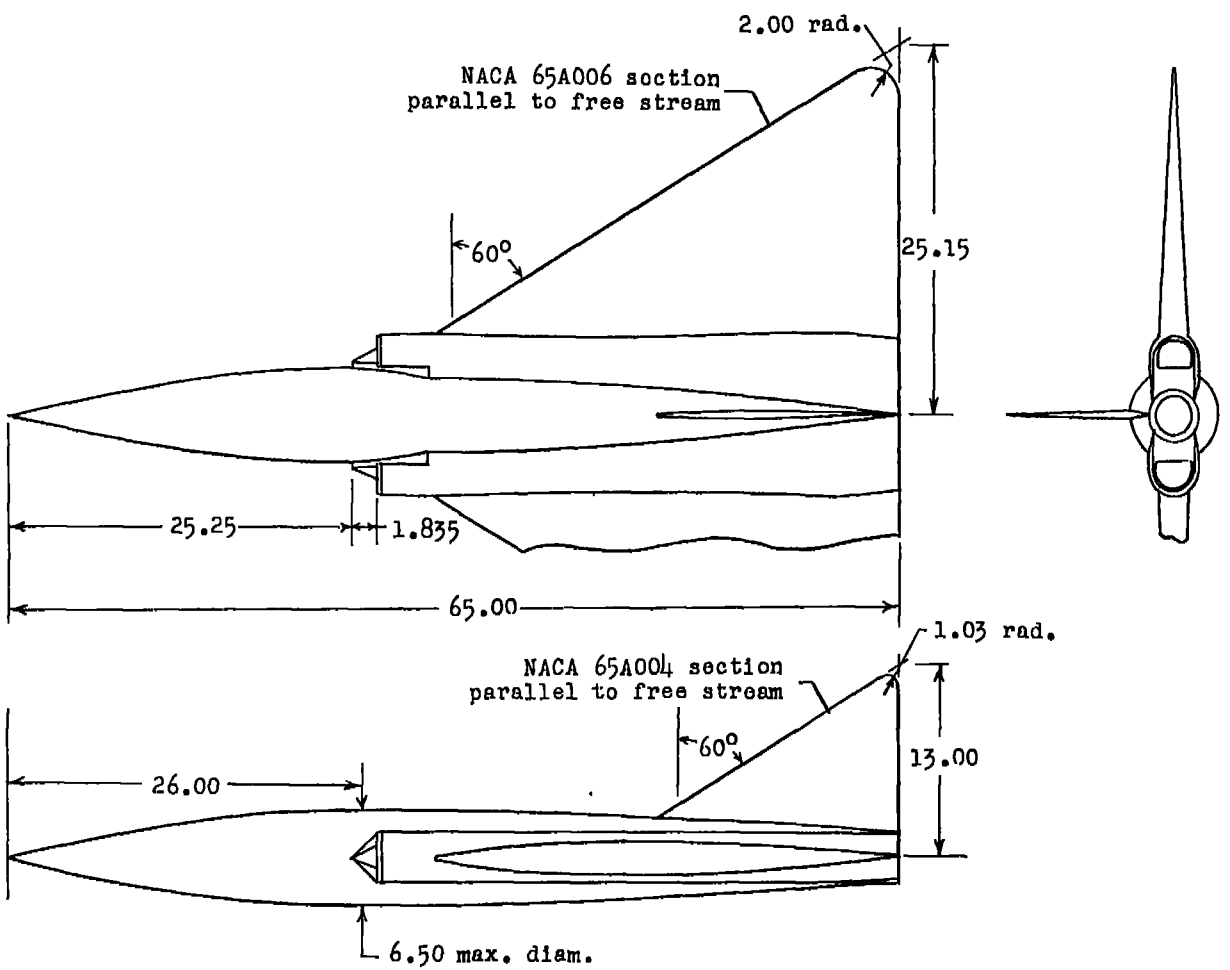

(a) Model 1.

Figure 2.- General arrangement of models. All dimensions in inches, except as noted.

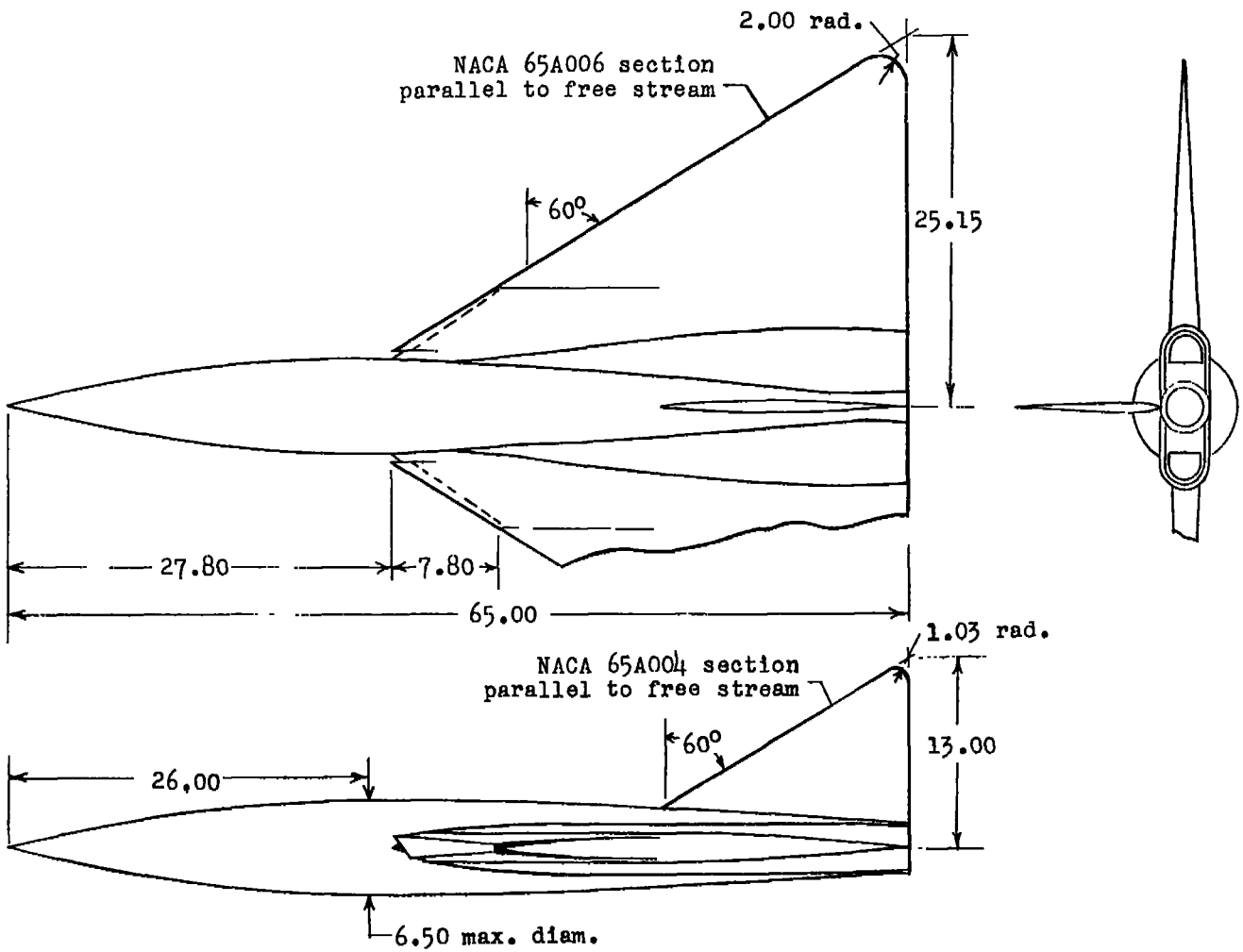

(b) Model 2.

Figure 2.- Concluded.

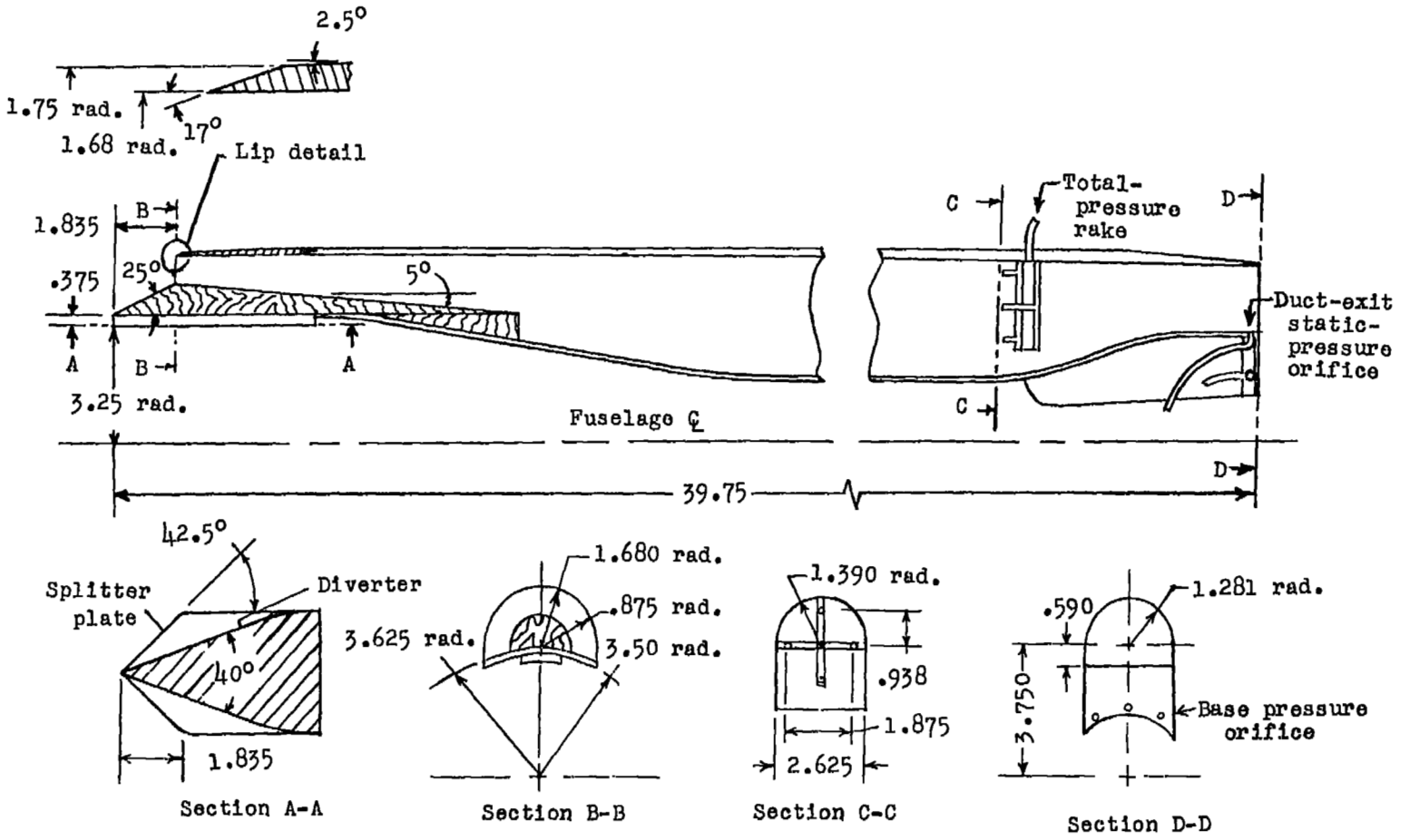

(a) Model 1.

Figure 3.- Details of inlet and ducting. All dimensions are in inches, except as noted.

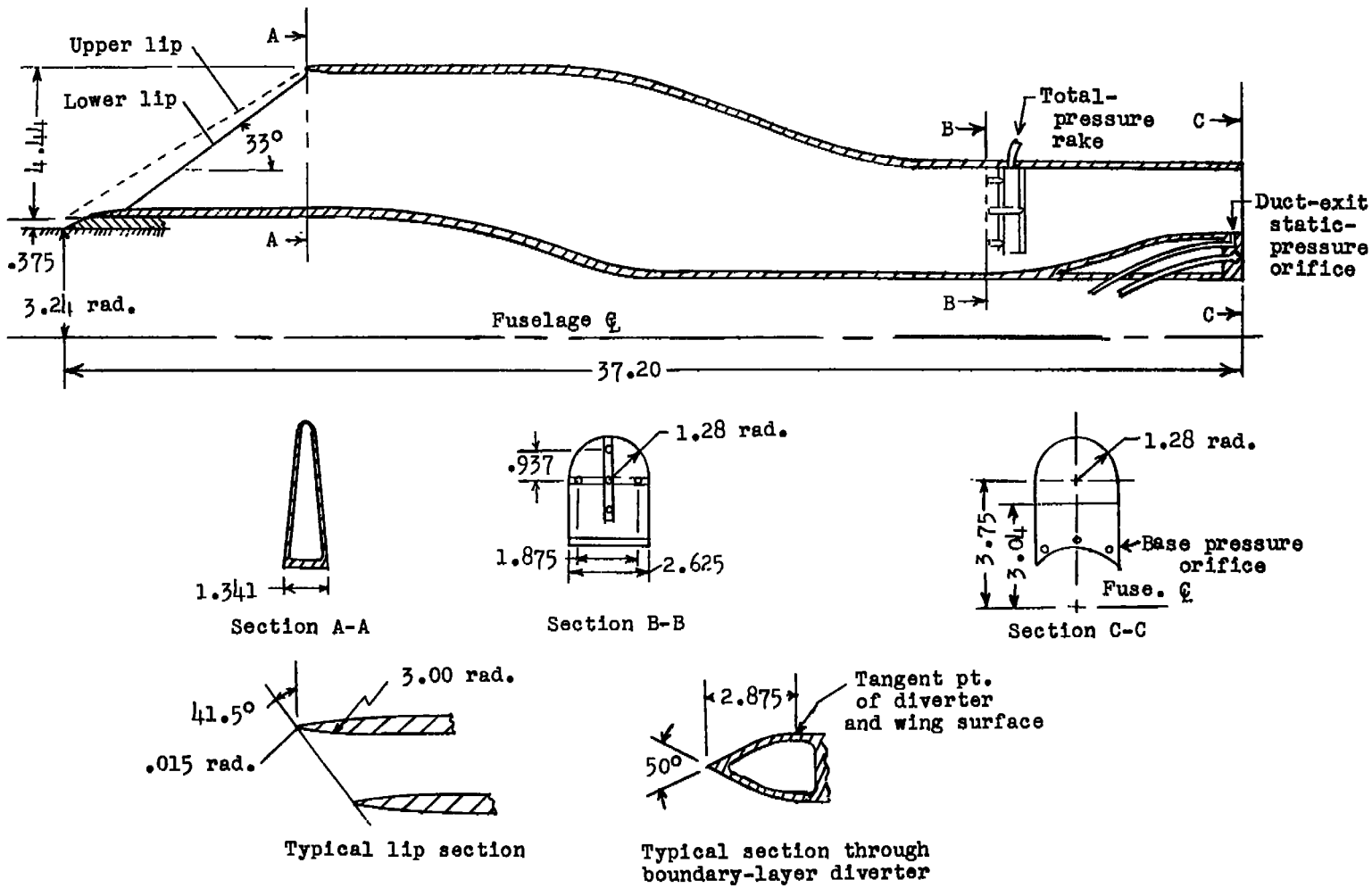

(b) Model 2.

Figure 3.- Concluded.

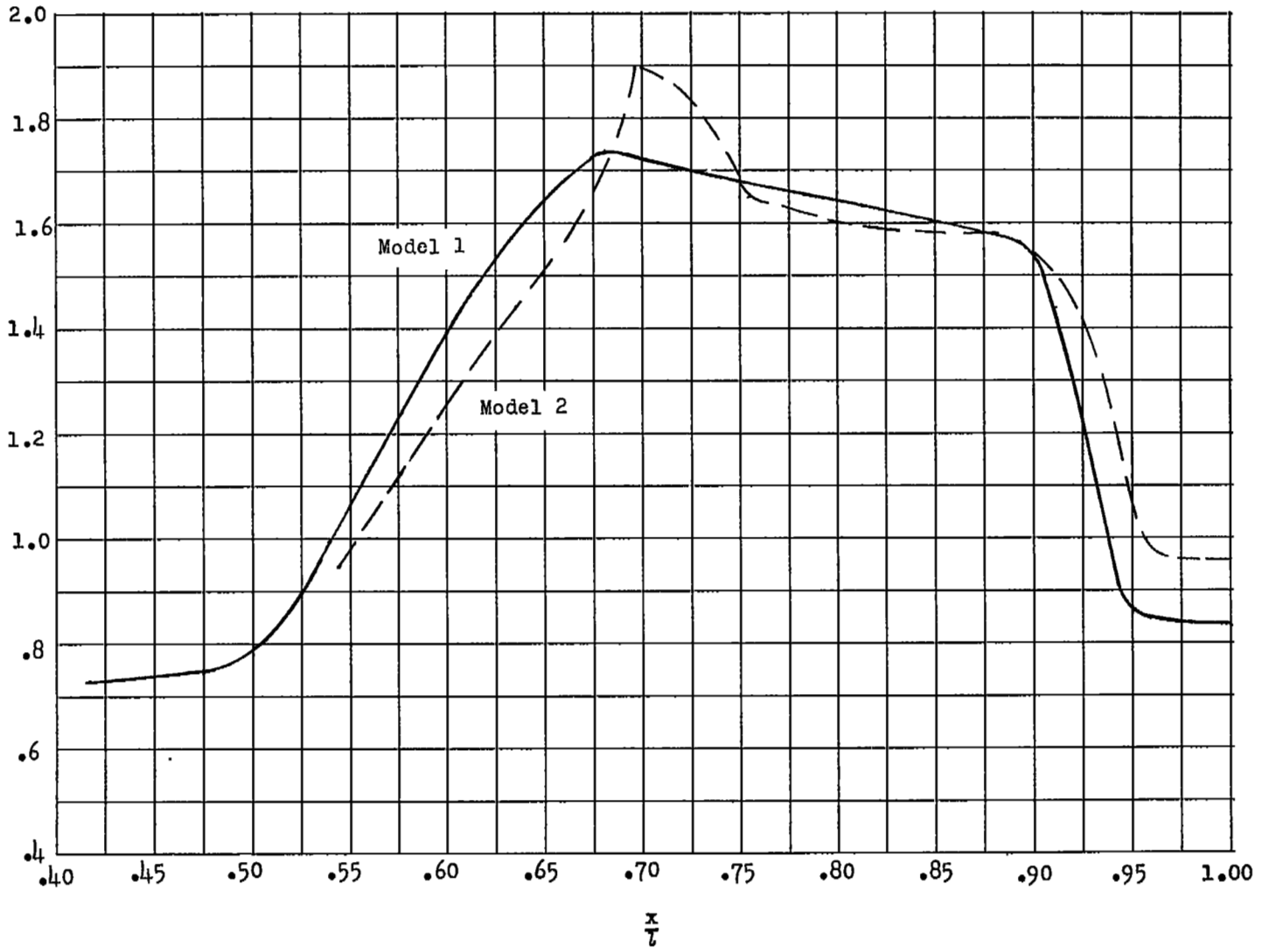

Figure 4.- Variation of duct cross-sectional area with model length.

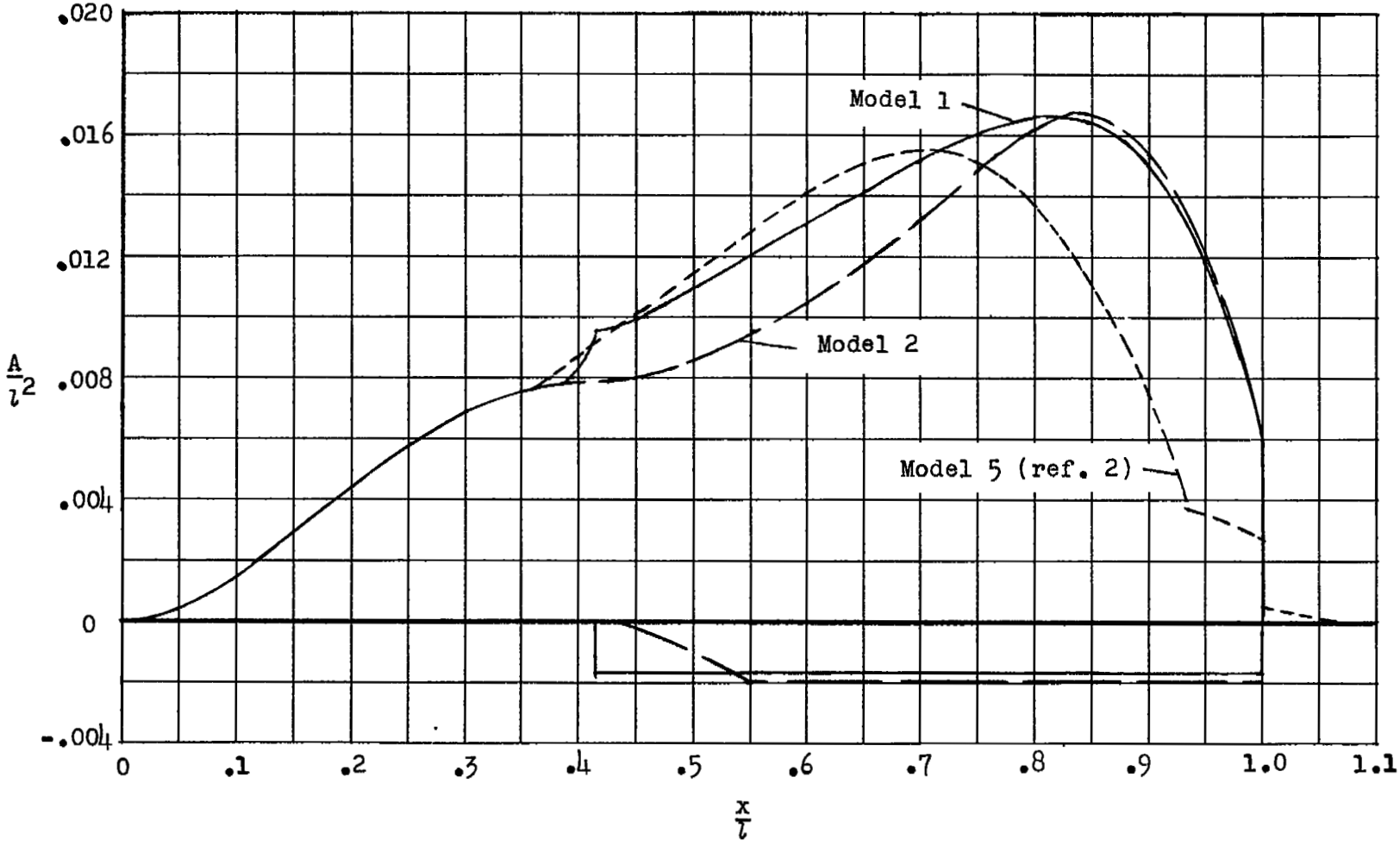

Figure 5.- Longitudinal area distribution of models. The area deducted for the mass-flow rate is shown at the bottom of the figure.

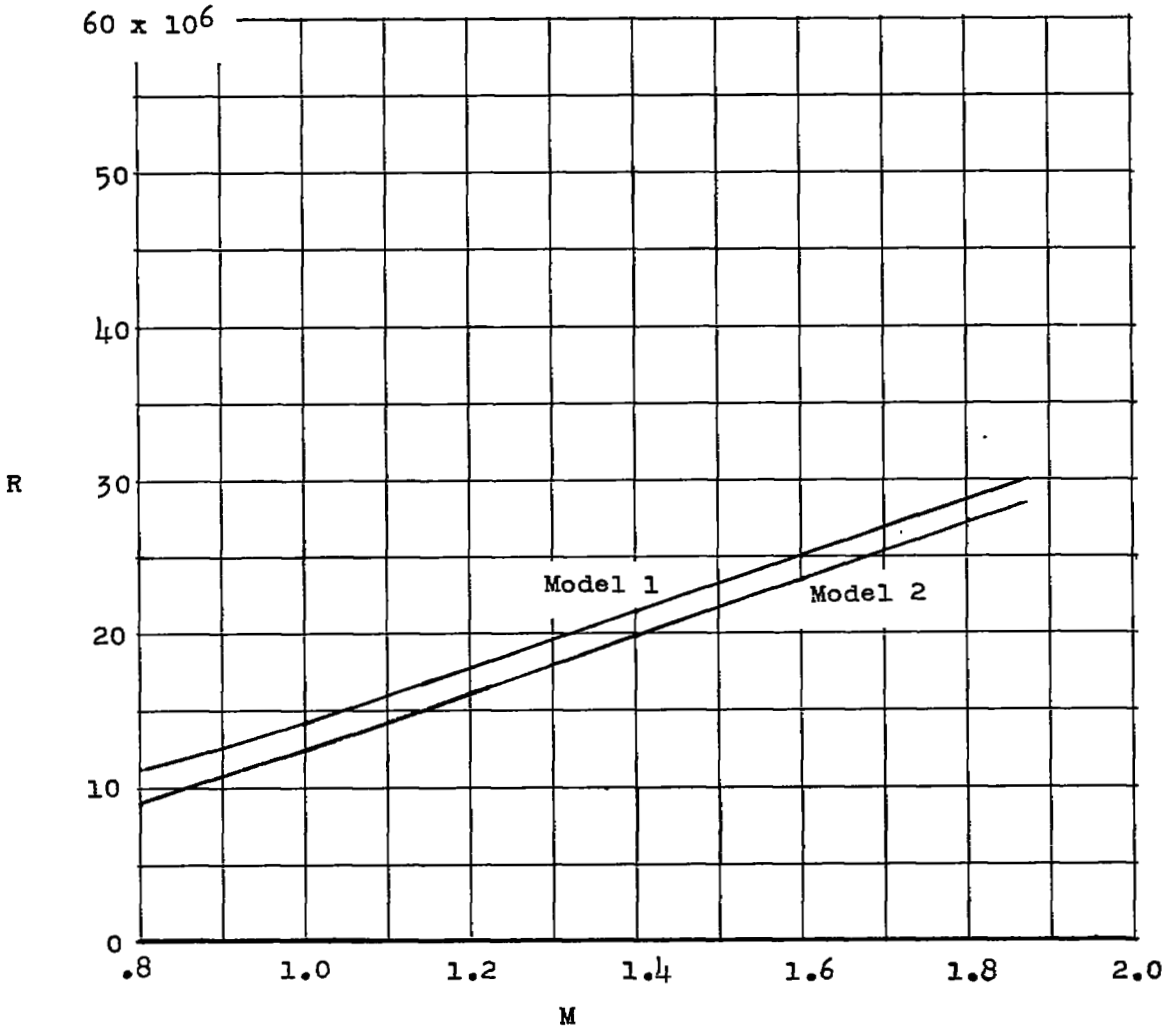

Figure 6.- Flight Reynolds numbers, based on mean aerodynamic chord of 2.42 feet, as a function of Mach number.

[redacted]

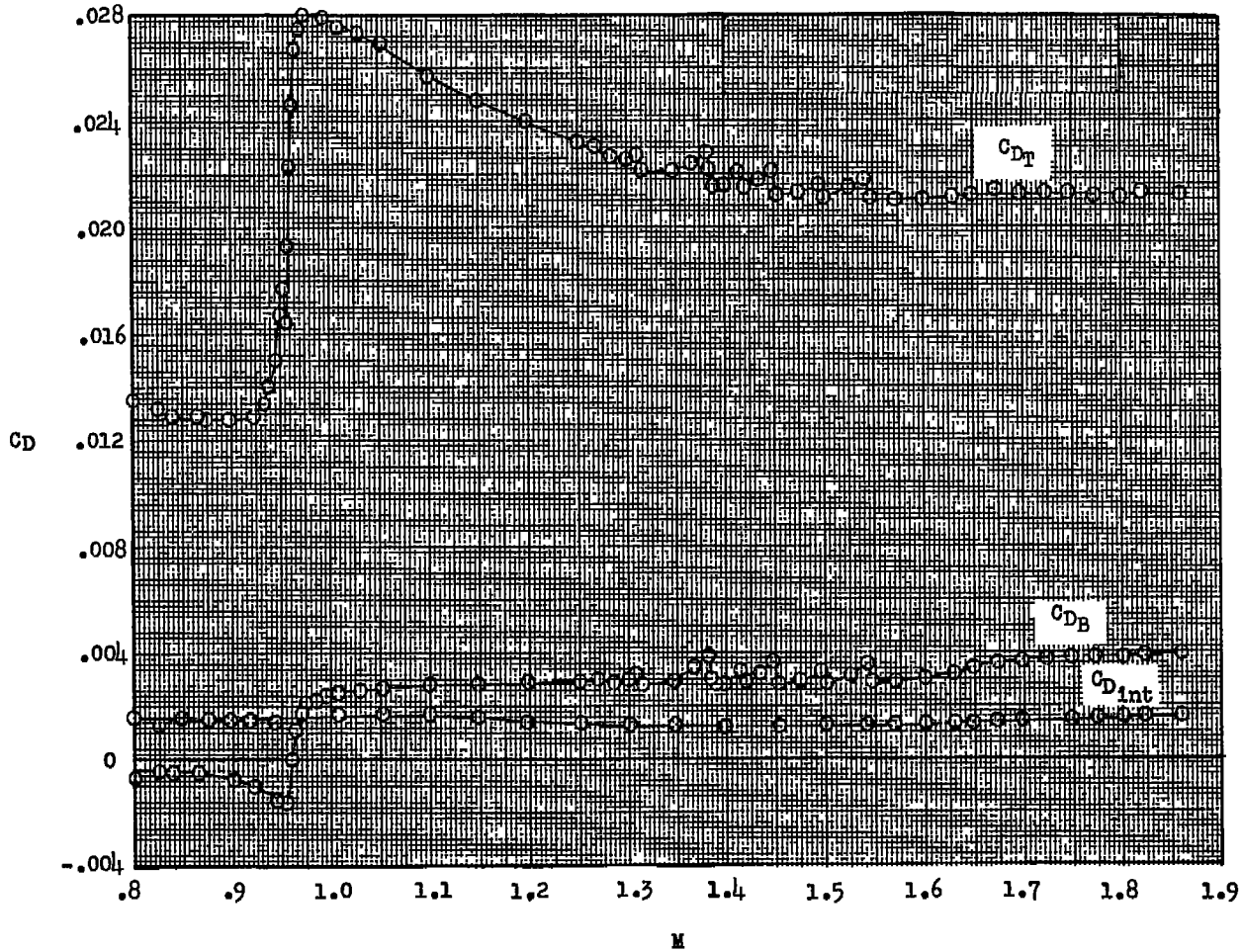

(a) Model 1.

Figure 7.- Total, internal, and base drag coefficients as a function of Mach number.

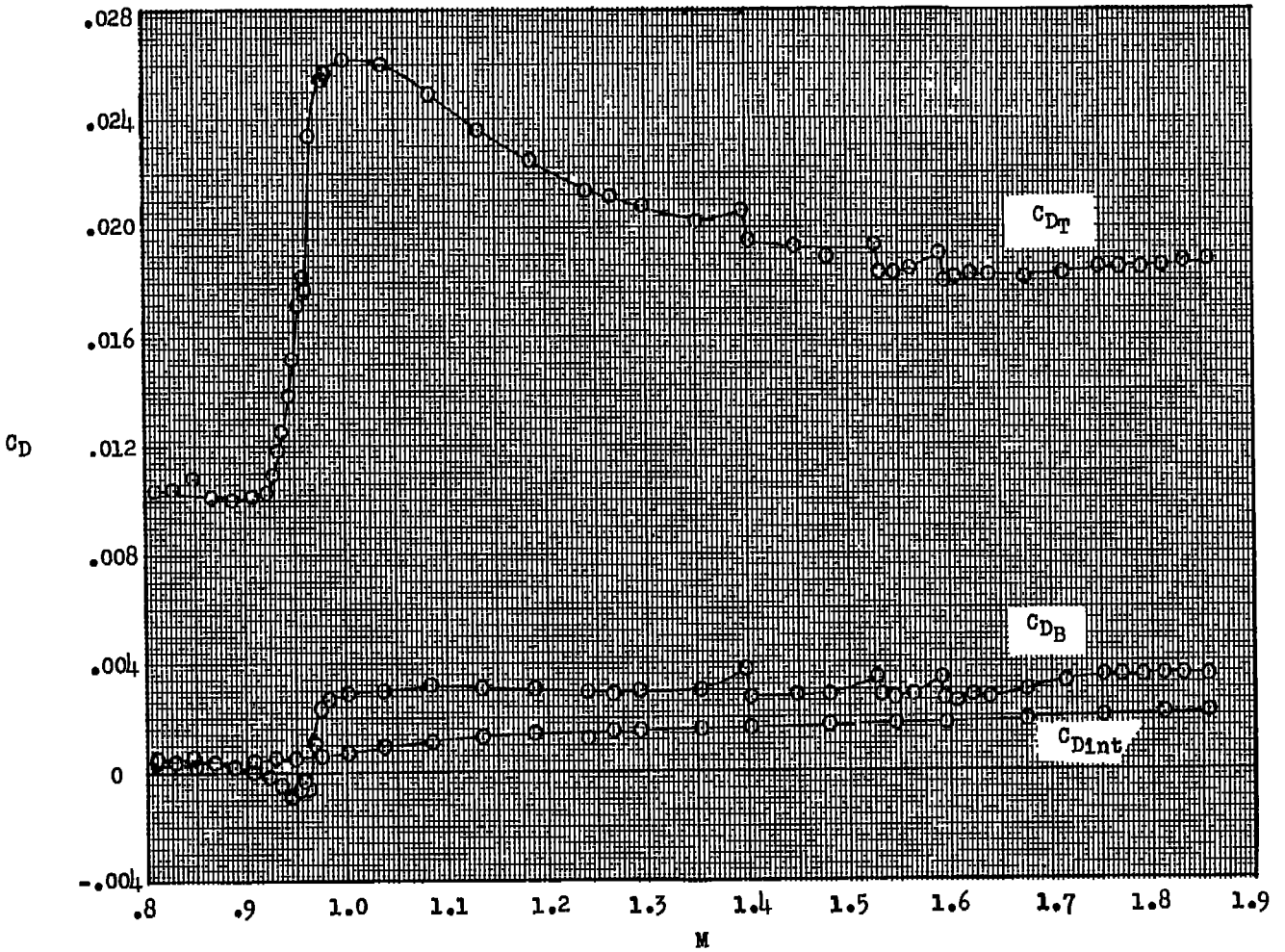

(b) Model 2.

Figure 7.- Concluded.

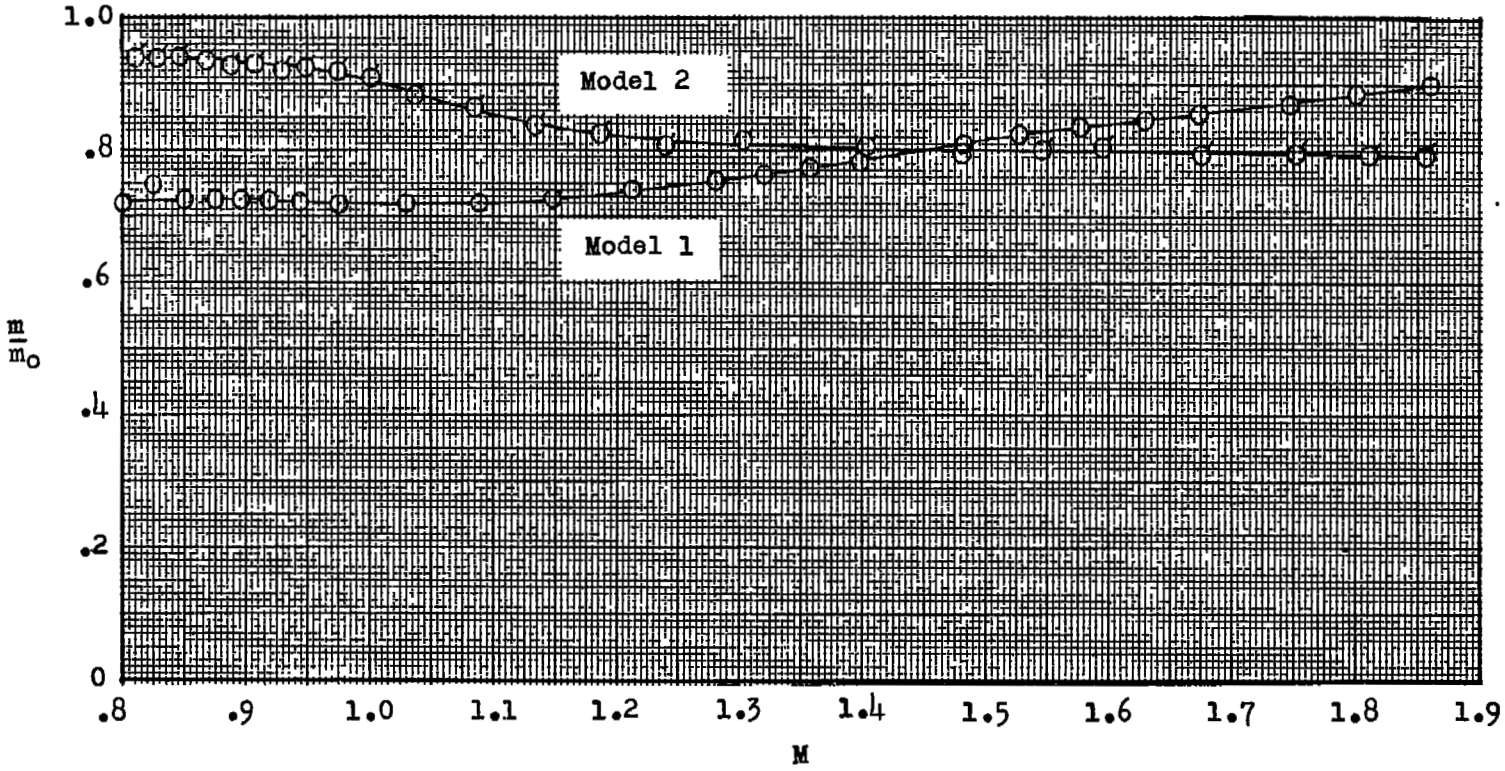

Figure 8.- Mass-flow ratios of models as a function of Mach number.

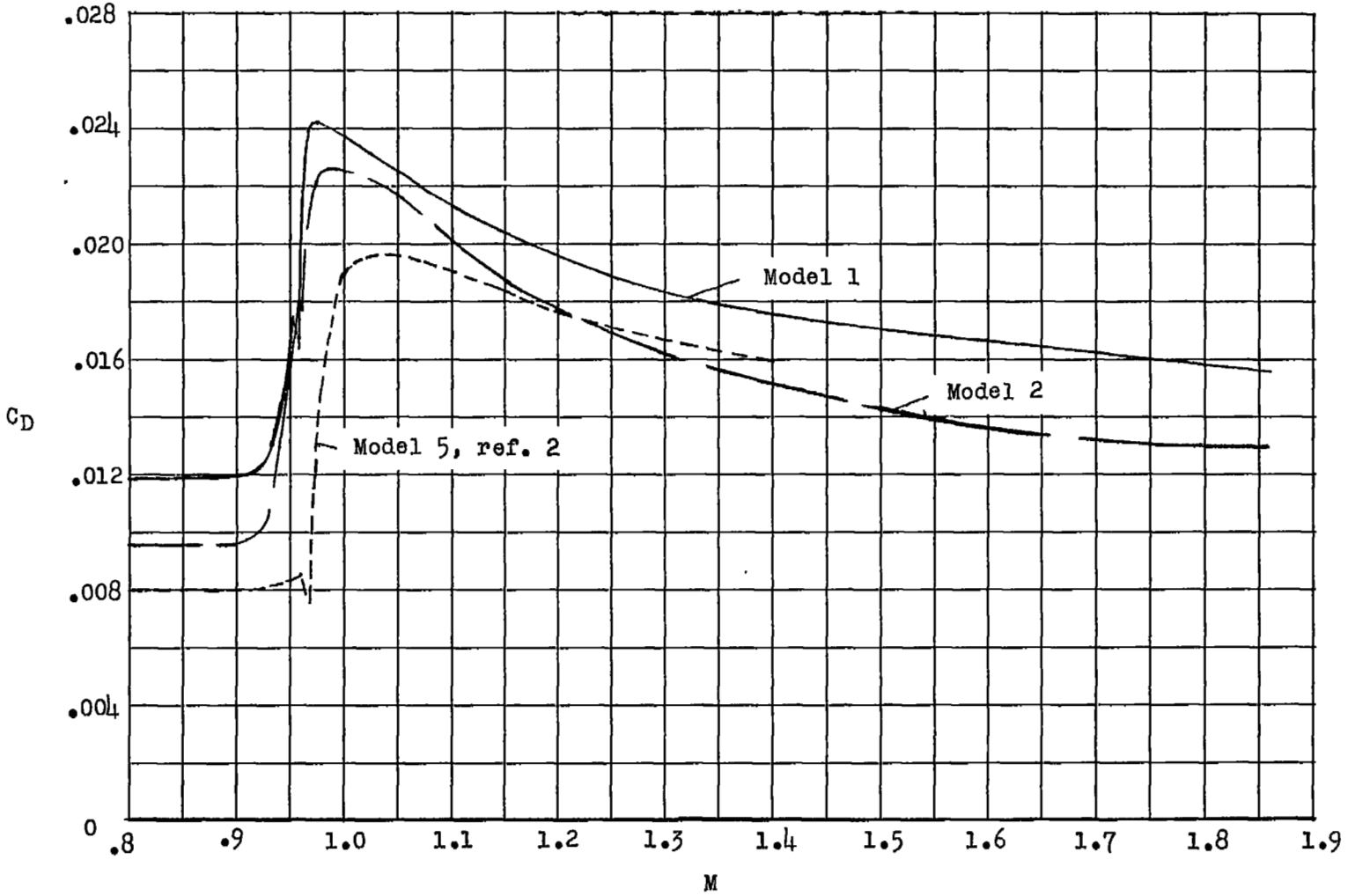

Figure 9.- External drag coefficient as a function of Mach number.